Relationship between constraining fields and effective fields in constrained density functional theory calculations for spin dynamics

Marian Arale Brännvall, Björn Alling, and Rickard Armiento
Department of Physics, Chemistry and Biology, Linköping University, 581 83 Linköping, Sweden

(Received 25 March 2025; revised 29 January 2026; accepted 3 February 2026; published 24 February 2026)

For density functional theory (DFT) based adiabatic spin dynamics, we investigate the relationship between the effective fields driving the dynamics of the atomic magnetic moments and the constraining fields used to enforce a specific noncollinear magnetic configuration. We revisit a derivation and a numerical comparison by Streib *et al.* [Phys. Rev. B **102**, 214407 (2020)] suggesting that the effective field from the energy gradient with respect to the magnetic moment direction and the constraining fields differ for systems with mean-field terms in the Hamiltonian, which they extended to include DFT. We find that a derivation focused on the DFT case clarifies what quantities to extract from the computational software to best represent the two fields. In particular, the definition of the magnetic moment magnitude must be consistent when making the comparison. This reestablishes the relationship of the two fields as having equal amplitude but opposite directions, in agreement with several earlier works. We also show that the constraining fields can be rescaled to reflect the correct field acting on the full, physically meaningful magnetic moment, rather than on the reduced moment used for numerical stability. Our numerical investigation is extended beyond the original case of an iron dimer to supercells of body-centered cubic iron in both ferromagnetic and disordered magnetic backgrounds, which further supports our conclusions.

DOI: 10.1103/nwd8-nsk3

I. INTRODUCTION

An accurate theoretical description of the dynamics of magnetic systems is essential for advancing our understanding of a wide range of phenomena and technologies. In ultrafast magnetism, for instance, a precise understanding of magnetic switching and domain wall motion holds the potential to make magnetic data storage faster and more energy efficient [1–5]. Similarly, the development of spintronic devices relies on detailed theoretical insights, where the dynamics of magnetic skyrmions are of particular interest. Investigating the dynamics of spins within these skyrmions is essential for understanding, e.g., their response to temperature and external magnetic fields [5,6]. In addition to technological applications, spin dynamics combined with molecular dynamics has become an important tool for modeling magnetic materials at elevated temperatures. This approach enables the study of magnetic phase transitions, the interplay between structural and magnetic transitions, and their phase stability [7–11]. However, achieving an accurate theoretical description remains a significant challenge, as magnetism is a collective phenomenon that emerges from the intricate interactions between the particles in the system.

Antropov *et al.* introduced a general *ab initio* approach to spin dynamics [7,8], which adiabatically separates the propagation of the directions and magnitudes of the magnetic moments, treating the directions as the slower degrees of freedom. In this approach, the effective fields driving the spin dynamics are calculated using spin-polarized density functional theory (SDFT) and are subsequently used to dynamically evolve the directions of the magnetic moments. Specifically, the effective fields generate torques acting on the magnetic moments when these are in a nonequilibrium state, guiding their evolution over time. However, Stocks *et al.* argued that since standard SDFT is a ground-state theory, nonequilibrium spin states are usually not accessible through this formulation [12]. One way of gaining access to the nonequilibrium spin states is by using time-dependent SDFT (TD-SDFT), which incorporates the time evolution of the spin density [13,14]. However, this approach is computationally expensive since the time steps of the electronic dynamics in TD-SDFT are of the order of attoseconds while the relevant rotational timescale of the magnetic moments is in the range of femto- to picoseconds. An alternative, used in several works, is to apply constrained ground state DFT with local constraining fields on the magnetic moments to enforce that a particular noncollinear configuration becomes the quasiequilibrium [12,15–18]. Edwards [16] and Stocks *et al.* [12] found that in this approach the field to use for the torque evolving the magnetic moment over time is precisely the negative of the constraining field needed to keep the moment fixed, that is, the effective field and the constraining fields have equal magnitude and opposite directions.

Published by the American Physical Society under the terms of the Creative Commons Attribution 4.0 International license. Further distribution of this work must maintain attribution to the author(s) and the published article's title, journal citation, and DOI. Funded by Bibsam.

Streib *et al.* recently argued that this equality does not hold in general for systems described by Hamiltonians with mean-field parameters [19]. They extended the result to SDFT based on the difference between the full electronic and the auxiliary Kohn-Sham Hamiltonians, but did not elaborate on the reason for the difference to the prior results for SDFT [12,16]. A direct comparison between the works is not straightforward in part because the derivation by Streib *et al.* was made via mean-field Hamiltonians, while DFT is different from typical mean field theories by being based on an exact formalism approximated by functionals. They also presented a numerical investigation showing a discrepancy between the fields for an iron dimer, both for a mean-field tight-binding model and for quantities extracted from constrained SDFT calculations made with the Vienna *ab initio* simulation package (VASP) [20–23]. However, we will discuss in the following which precise quantities best represent the two fields in this comparison. While the tight-binding model was further explored in subsequent works [24–26], we are not aware of further investigations related to the results for SDFT.

In this work, we reexamine the relationship between the constraining and effective fields strictly within the context of SDFT. We first reiterate in detail an updated version of the analytical derivation of Edwards [16] and then revisit the numerical investigation of the iron (Fe) dimer by Streib *et al.* [19], which we also extend to body-centered cubic (bcc) Fe in both ferromagnetic and disordered magnetic backgrounds. We use our analytical results to clarify which quantities to extract from the computations, especially for the magnitude of the magnetic moment and in relation to the electron g factor. These insights enable us to reestablish the equal but opposite nature of the effective and constraining fields across all the test cases.

Consequently, our paper reconfirms prior works relying on this relationship in SDFT [12,15–18] and the technique to perform *ab initio* spin dynamics, within the adiabatic approximation, by using the negative of the constraining fields calculated by SDFT as the effective fields driving the dynamics as described by, for instance, the Landau-Lifshitz-Gilbert equation of motion [27]. These findings also justify the use of constraining fields as physically relevant quantities in other contexts, e.g., as DFT-based training data for machine learning models for predicting the magnetic torques, as has recently been done in the work by Yang *et al.* [28].

In Sec. II, the adiabatic *ab initio* spin dynamics approach by Ref. [8] and the constraining method introduced by Ma and Dudarev [18] are described. In Sec. III, the analytical and numerical results are presented and discussed. Lastly, in Sec. IV, the conclusions are summarized.

II. BACKGROUND

A. Adiabatic *ab initio* spin dynamics

The dynamics of the spin density can be described using *ab initio* spin dynamics within the adiabatic approximation as introduced by Antropov *et al.* [7,8]. This approach is based on electronic structure calculations and can be implemented using DFT. The adiabatic approximation involves separating spin degrees of freedom according to their distinct timescales, specifically decoupling the dynamics of the direction of the spin density from changes in its magnitude and in the charge density. The former is slower than the latter. The charge density and the magnitude of the spin density are considered in a quasiequilibrium state, where the direction of the spin density is held fixed. This is similar to the Born-Oppenheimer approximation where the nuclei motion is separated from the motion of the electrons. For systems where the spatially varying spin density, $\mathbf{m}(\mathbf{r})$, can be approximated as collinear within a sphere encapsulating an atom, the rigid-spin approximation may be applied when rotating atomic magnetic moments. A unit vector at site I, $\mathbf{e}_I$, is then associated to such an atomic sphere, Ω_I, and the atomic magnetic moment is given by

$$\mathbf{M}_I = \int_{\Omega_I} \mathbf{m}(\mathbf{r}) d^3r = M_I \mathbf{e}_I, \tag{1}$$

where M_I is the magnitude of the atomic magnetic moment. The equation of motion of the direction of the atomic magnetic moment is given by

$$\frac{d\mathbf{e}_I}{dt} = \gamma \mathbf{e}_I \times \mathbf{B}_I^{\text{eff}}, \tag{2}$$

where $\gamma = -g\mu_B/\hbar$ with the electron spin g factor ($g \approx 2$), μ_B is the Bohr magneton, and $\mathbf{B}_I^{\text{eff}}$ is the effective magnetic field at site I,

$$\mathbf{B}_I^{\text{eff}} = -\frac{1}{M_I}\frac{\partial E}{\partial \mathbf{e}_I}, \tag{3}$$

which depends on both internal and external interactions [8].

B. Constraining fields

The direction of the spin density depends directly on the electronic structure. To stabilize an arbitrary noncollinear magnetic configuration, which is typically not a ground state in SDFT, it is necessary to introduce constraints to enforce a particular configuration. One method for constraining the directions and signs of the magnetic moments was developed by Ma and Dudarev [18]. In this approach, the directions of the magnetic moments are constrained, but their magnitudes are allowed to change; spin flips are, however, prevented. This is achieved by introducing a penalizing term that is minimized when the magnetic moments are in the desired directions, $\mathbf{e}_I^*$,

$$E = E_0 + E_{\text{p}} = E_0 + \lambda \sum_I \left(M_I^F - \mathbf{e}_I^* \cdot \mathbf{M}_I^F\right), \tag{4}$$

where E_0 and E_{p} are the internal total energy of the system and the penalty energy, respectively; M_I^F is the magnitude of the atomic magnetic moment $\mathbf{M}_I^F$ and λ is a parameter determining the strength of the penalty term. The magnetic moment is defined differently from Eq. (1) as

$$\mathbf{M}_I^F = \int_{\Omega_I} \mathbf{m}(\mathbf{r}) F_I(|\mathbf{r} - \mathbf{r}_I|) d^3r, \tag{5}$$

where $F_I(|\mathbf{r} - \mathbf{r}_I|)$ is a function that decreases smoothly towards zero at the edge of the atomic sphere to make the constrained calculations numerically robust. The penalty term introduces constraining fields within the spheres given by

$$\mathbf{B}^{\text{con}}(\mathbf{r}) = -\frac{\delta E_p}{\delta \mathbf{m}(\mathbf{r})}. \tag{6}$$

It can be shown that in the limit of $\lambda \to \infty$ the penalty energy goes to zero while $\mathbf{B}^{\text{con}}$ converges to a finite value [18].

III. RESULTS AND DISCUSSION

In this section, the analytical results showing the relation between the constraining field of a magnetic moment and the energy gradient with respect to moment rotation are presented within density functional theory. Numerical results from an Fe dimer and supercells of bcc Fe are shown to support the analytical findings.

A. Analytical results

As a starting point, we examine the effect of including a penalty term that constrains the direction of the magnetization density in the total energy functional within the general non-collinear spin-polarized extension of DFT introduced by von Barth and Hedin [29]. The total energy functional in DFT is then given by [15]

$$E_{\text{tot}} = T_0 + \int v_{\text{ext}}(\mathbf{r}) n(\mathbf{r}) d\mathbf{r} + \iint \frac{n(\mathbf{r}) n(\mathbf{r}')}{|\mathbf{r} - \mathbf{r}'|} d\mathbf{r}\, d\mathbf{r}' + E_{\text{xc}} + E_{\text{p}} \equiv E_0 + E_{\text{p}}, \tag{7}$$

where T_0 is the kinetic energy of the noninteracting particles, $v_{\text{ext}}(\mathbf{r})$ the external potential, $n(\mathbf{r})$ is the charge density, E_{xc} is the exchange-correlation energy functional, and E_{p} is the penalty term. The sum of the first four terms is denoted E_0. In SDFT, spinors are attached to the wave functions, which requires the Hamiltonian to be a 2×2 matrix. By introducing this spin dependence, the scalar charge density is replaced by the spin-density matrix, $\tilde{n}(\mathbf{r})$ [29,30]. The elements of $\tilde{n}(\mathbf{r})$ are given by

$$n_{\beta\alpha}(\mathbf{r}) = \sum_{i=1}^{N} \psi_{i\beta}(\mathbf{r}) \psi^*_{i\alpha}(\mathbf{r}), \tag{8}$$

where $\alpha, \beta \in \{\uparrow, \downarrow\}$ are the spin indices, $\psi_{i\alpha}(\mathbf{r})$ denotes the spin-α component of the single-particle wave function, given as a two-component spinor, $\psi_i(\mathbf{r}) = [\psi_{i\uparrow}(\mathbf{r}), \psi_{i\downarrow}(\mathbf{r})]$, of the ith particle, and the sum runs over all particles. Within this framework, the traditional DFT condition of the total energy, E_{tot}, being stationary with respect to variations in the charge density is replaced with it being stationary with respect to variations in $\tilde{n}(\mathbf{r})$ (to be understood as the variation with respect to each individual matrix element). The variation of Eq. (7) can be expressed, using the chain rule, as

$$\frac{\delta E_{\text{tot}}[n, \mathbf{m}]}{\delta \tilde{n}(\mathbf{r})} = \frac{\delta E_{\text{tot}}[n, \mathbf{m}]}{\delta n(\mathbf{r})} \frac{\delta n(\mathbf{r})}{\delta \tilde{n}(\mathbf{r})} + \frac{\delta E_{\text{tot}}[n, \mathbf{m}]}{\delta \mathbf{m}(\mathbf{r})} \frac{\delta \mathbf{m}(\mathbf{r})}{\delta \tilde{n}(\mathbf{r})} = 0. \tag{9}$$

We find that

$$\frac{\delta n(\mathbf{r})}{\delta \tilde{n}(\mathbf{r})} = \mathbf{I}_{2\times 2}, \quad \frac{\delta \mathbf{m}(\mathbf{r})}{\delta \tilde{n}(\mathbf{r})} = \hat{\boldsymbol{\sigma}}, \tag{10}$$

where $\mathbf{I}_{2\times 2}$ is the 2×2 identity matrix and $\hat{\boldsymbol{\sigma}}$ is the vector of Pauli matrices. The effective potential in which the independent Kohn-Sham particles move is, consequently, given by

$$\mathbf{v}^{\text{eff}}(\mathbf{r}) = \left[v_{\text{ext}}(\mathbf{r}) + 2 \int \frac{n(\mathbf{r}')}{|\mathbf{r} - \mathbf{r}'|} d\mathbf{r}' + \mu_{\text{xc}}(\mathbf{r}) \right] \mathbf{I}_{2\times 2} - \hat{\boldsymbol{\sigma}} \cdot \mathbf{B}_{\text{xc}}(\mathbf{r}) - \hat{\boldsymbol{\sigma}} \cdot \mathbf{B}_{\text{con}}(\mathbf{r}), \tag{11}$$

where we assume that the penalty energy depends only on the spin density, i.e., $E_{\text{p}} = E_{\text{p}}[\mathbf{m}]$, and use the notations

$$\mu_{\text{xc}} = \frac{\delta E_{\text{xc}}}{\delta n(\mathbf{r})}, \quad \mathbf{B}_{\text{xc}}(\mathbf{r}) = -\frac{\delta E_{\text{xc}}}{\delta \mathbf{m}(\mathbf{r})}, \quad \mathbf{B}_{\text{con}}(\mathbf{r}) = -\frac{\delta E_{\text{p}}}{\delta \mathbf{m}(\mathbf{r})}. \tag{12}$$

Note that the penalty term is part of the effective potential. The Kohn-Sham equations are given by

$$\sum_{\beta} [\delta_{\alpha\beta}(-\nabla^2 + v_0(\mathbf{r})) - (\hat{\boldsymbol{\sigma}} \cdot \mathbf{B}_{\text{xc}}(\mathbf{r}))_{\alpha\beta} - (\hat{\boldsymbol{\sigma}} \cdot \mathbf{B}_{\text{con}}(\mathbf{r}))_{\alpha\beta} - \delta_{\alpha\beta}\varepsilon_i] \psi_{i\beta} = 0, \tag{13}$$

together with Eq. (12), for all $\alpha \in \{\uparrow, \downarrow\}$, where ∇^2 is the Laplacian operator and

$$v_0(\mathbf{r}) = v^{\text{ext}}(\mathbf{r}) + 2 \int \frac{n(\mathbf{r}')}{|\mathbf{r} - \mathbf{r}'|} d\mathbf{r}' + \mu_{\text{xc}}(\mathbf{r}). \tag{14}$$

The above derivation shows how the penalty term contributes with a constraining field in the Kohn-Sham equations. Next, we examine the impact of rotating a magnetic moment on the energy functional, following the derivation by Edwards [16]. As mentioned previously, the variation is made with respect to the spin-density matrix. From Eq. (9) it is seen that this can be reformulated as E_{tot} being stationary with respect to independent variations in the charge and spin densities,

$$\frac{\delta E_{\text{tot}}}{\delta n(\mathbf{r})} = 0, \quad \frac{\delta E_{\text{tot}}}{\delta \mathbf{m}(\mathbf{r})} = 0. \tag{15}$$

The variation with respect to spin density, with E_{tot} given by Eq. (7), results in

$$\frac{\delta E_0}{\delta \mathbf{m}(\mathbf{r})} = -\frac{\delta E_{\text{p}}}{\delta \mathbf{m}(\mathbf{r})}, \tag{16}$$

where the right-hand side is the constraining field, $\mathbf{B}_{\text{con}}(\mathbf{r})$, introduced in the Kohn-Sham equations in Eq. (13). Subsequently, Eq. (16) can be rewritten as

$$\delta E_0 = \mathbf{B}_{\text{con}}(\mathbf{r}) \cdot \delta \mathbf{m}(\mathbf{r}). \tag{17}$$

Assuming a rigid-spin rotation of the spin density within the atomic sphere associated with lattice site I, the small rotation $\delta\theta_I$ of the magnetic moment around, e.g., the y axis is given by

$$\delta \mathbf{M}_I = \delta\theta_I \hat{\mathbf{y}} \times \mathbf{M}_I \tag{18}$$

with $\mathbf{M}_I$ defined as in Eq. (1). Combining Eqs. (17) and (18), it follows that

$$\delta E_0 = \mathbf{B}_I^{\text{con}} \cdot \delta\theta_I \hat{\mathbf{y}} \times \mathbf{M}_I = \delta\theta_I \hat{\mathbf{y}} \cdot \mathbf{M}_I \times \mathbf{B}_I^{\text{con}} \Rightarrow$$
$$\frac{\delta E_0}{\delta\theta_I} = \hat{\mathbf{y}} \cdot \mathbf{M}_I \times \mathbf{B}_I^{\text{con}}, \tag{19}$$

where $\mathbf{B}_I^{\text{con}}$ is the constraining field associated with site I. Since $\mathbf{M}_I$ and $\mathbf{B}_I^{\text{con}}$ are perpendicular (when only constraining the direction) and, for simplicity, considered to be completely in the x-z plane, we have $\hat{\mathbf{y}} \cdot \mathbf{M}_I \times \mathbf{B}_I^{\text{con}} = M_I B_I^{\text{con}}$, which leads to

$$\frac{1}{M_I}\frac{\delta E_0}{\delta\theta_I} = B_I^{\text{con}}. \tag{20}$$

Within the rigid-spin approximation, when varying only the angle θ_I, the effective magnetic field at site I is given by Eq. (3) as

$$B_I^{\text{eff}} = -\frac{1}{M_I}\frac{\partial E_0}{\partial\theta_I}. \tag{21}$$

Combining Eqs. (20) and (21) leads to the final expression:

$$B_I^{\text{eff}} = -B_I^{\text{con}}. \tag{22}$$

In SDFT, the effective field, as given by the energy gradient, is exactly equal to the negative of the constraining field used to enforce a specific direction for the magnetic moment. Note that this derivation is independent of the choice of the exchange-correlation approximation.

B. Numerical results

1. Computational details

The DFT calculations are performed using the Vienna *ab initio* simulation package (VASP) [20–23] with projector augmented-wave potentials (PAW) [31,32] and the Perdew-Burke-Ernzerhof (PBE) generalized gradient approximation (GGA) for approximating the exchange-correlation functional [33]. Calculations are performed for an Fe dimer and a supercell consisting of a $3 \times 3 \times 3$ replication of the conventional bcc unit cell, with 54 Fe atoms in total. In all cases, the Fe 4*s* and 3*d* electrons are treated as valence electrons. For the iron dimer, the energy cutoff is set to 600 eV. A Monkhorst-Pack grid with a single k point is used [34]. The two atoms are 2 Å apart in a $8 \times 8 \times 8$ Å^3 simulation box and the Wigner-Seitz radius is 1 Å. For the supercell, both a ferromagnetic (FM) background and a magnetically disordered background are considered. The magnetic disorder is simulated using the disordered local moment (DLM) approach [35,36]. The lattice constant is 2.83 Å, the energy cutoff is 500 eV, and a Monkhorst-Pack $5 \times 5 \times 5$ and $3 \times 3 \times 3k$-point grid is used for the FM and DLM background, respectively. The Wigner-Seitz radius is in this case 1.302 Å, corresponding to the radius of the projector augmented-wave potential sphere for Fe in VASP.

To obtain the magnetic moments, we use the projection method implemented in VASP, which is based on the projector functions within the PAW method. In both the dimer and supercells, the magnetic moment of one of the atoms is rotated in steps of 0.008 rad to represent an infinitesimal change in the angle. The remaining magnetic moments are held fixed in direction and sign, but not in magnitude. To constrain the magnetic moment directions, the method by Ma and Dudarev is used with $\lambda = 50\,\text{eV}/\mu_\text{B}$ [18]. In the DLM background, the rotational axis is chosen to be the cross product between the initial constraining field and the vector representing the rotated magnetic moment. The numerical derivative is computed using the centered difference approximation with function values at five equally spaced points: two points before and two points after the target point, along with the target point itself to minimize noise. Additionally, to smoothen the energy gradient curve further, the Savitzky-Golay filter is used [37] as implemented in the PYTHON package SCIPY [38].

2. Magnitude of the atomic magnetic moment

In Eq. (21), the energy gradient with respect to the rotation angle is scaled by the magnitude of the atomic magnetic moment.

When constraining the magnetic configuration in VASP, up to three different magnitudes for the magnetic moments can be given as output: (*i*) the scaled magnitude of Eq. (5) with a user-defined sphere Ω_I, (*ii*) the magnitude given by the integral of Eq. (1) where the sphere Ω_I is also defined by the user, and (*iii*) the magnitude given by integrating over the projector augmented-wave potential sphere; from now on, these magnitudes are referred to M_I^F, M_I^R, and M_I^{PAW}, respectively. The last case is only applicable when the projection method is chosen, which uses the projector functions provided by the PAW method to determine the atomic magnetic moments. Case (*ii*) can be made to match case (*iii*) by altering the user-defined Wigner-Seitz radius. The magnetic moment magnitude in case (*i*) will, however, differ from the other two due to the smoothening function, $F_I(|\mathbf{r} - \mathbf{r}_I|)$. Since the constraining fields are based on the scaled magnitudes of (*i*), this must be taken into account when comparing the left- and right-hand side of Eq. (20). Direct comparison with the constraining fields as given by VASP requires the energy gradient to be divided by M_I^F. In the following, we also show that the constraining field can be rescaled to match the effective field acting on the full magnetic moment, which we define as the M_I^{PAW} magnetic moment.

3. Fe dimer

We begin the numerical investigations with the same system as in Ref. [19], an Fe dimer, examining the left- and right-hand side of Eq. (20). The magnetic moments are initially aligned ferromagnetically in the z direction. One of the moments, $\mathbf{M}_I$, is rotated stepwise in the x-z plane until it forms an angle of 90° with the other magnetic moment. In Fig. 1, the two sides of Eq. (20) are plotted as functions of the angle; the energy gradient is divided by M_I^F in Eq. (5). The magnetic moment obtained from VASP is $M_I^F = 1.57\mu_B$. The constraining field B_I^{con} is taken directly from the output of VASP, i.e., no rescaling is done. For comparison, we have included the energy gradient field and the constraining field extracted from Fig. 2 in Ref. [19] as well as our attempt to recreate their results by the relation

$$-B_I^{\text{grad}} = \frac{g}{M_I^{\text{PAW}}}\frac{\partial E}{\partial\theta} \tag{23}$$

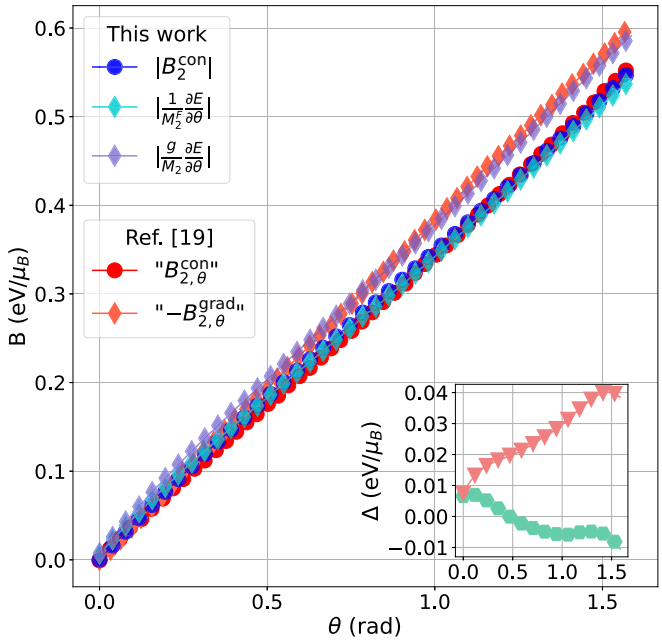


FIG. 1. Comparison of the constraining magnetic field and the effective magnetic field calculated as the energy derivative for the Fe dimer. Our constraining field (blue circles) and effective magnetic field (turquoise diamonds) based on Eq. (21) agree when using the magnetic moment magnitude M_I^F. Results extracted from Fig. 2 in Ref. [19] (red circles, orange diamonds) shows the discrepancy between the fields highlighted in that work. Recalculating the effective magnetic field of our data using Eq. (23) (representing our understanding of the quantity used for the orange diamonds) reproduces the same discrepancy with the constraining field (purple diamonds vs blue circles). The inset shows the difference between the two fields: $\Delta = |B_I^{\mathrm{eff}}| - |B_I^{\mathrm{con}}|$, where B_I^{eff} is given by either Eq. (21) [green hexagons] or (23) [orange triangles].

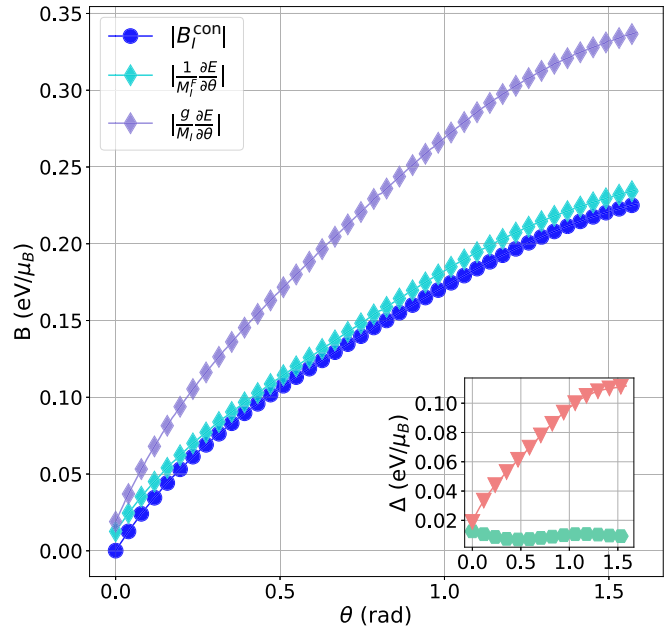


FIG. 2. Comparison of the constraining magnetic field and the effective magnetic field calculated as the energy derivative for the supercell of bcc Fe in ferromagnetic background. The constraining field (blue circles) and effective magnetic field (turquoise diamonds) based on Eq. (21), with the magnetic moment magnitude M_I^F, agree well. The effective magnetic field of our data but recalculated based on Eq. (23) shows a significant discrepancy (purple diamonds vs blue circles). The inset shows the difference between the two fields: $\Delta = |B_I^{\mathrm{eff}}| - |B_I^{\mathrm{con}}|$, where B_I^{eff} is given by either Eq. (21) [green hexagons] or (23) [orange triangles].

for the energy gradient, where $g \approx 2$. For the Fe dimer, $M_I^{\mathrm{PAW}} \approx 2.83\mu_B$. The inclusion of the g factor is discussed in Sec. III C. Equation (23) corresponds to the property denoted as $-B_{2,\theta}^{\mathrm{grad}}$ in Ref. [19].

4. Supercells of Fe

Figures 2 and 3 show the comparison between the energy gradient field and the constraining field in bcc supercells of 54 Fe atoms in ferromagnetic (FM) and disordered local moment (DLM) configurations, respectively. In the FM case, the atomic magnetic moments are all initially aligned in the z direction. One of the magnetic moments is subsequently rotated, stepwise, in the x-z plane until it is at a 90° angle relative to the surrounding magnetic moments. In this FM background, the scaled magnitude of the rotated magnetic moment from Eq. (5) is obtained from VASP as $1.64 > M_I^F > 1.47\mu_B$, where the magnitude decreases as the angle increases. The full magnetic moment within the PAW potential sphere is $2.18 > M_I^{\mathrm{PAW}} > 2.05\mu_B$.

The DLM background consists of atomic magnetic moments with random directions. This configuration is stabilized by constraining fields. One of the magnetic moments is then rotated around the axis in the direction of the cross-product between the initial constraining field and the magnetic moment vector, $\mathbf{B}_I^{\mathrm{con}} \times \mathbf{M}_I$. The angle is, thus, relative to the initial direction and not relative to the surrounding magnetic moments in the DLM case. The atomic magnetic moment is rotated until it is 90° away from the initial direction. The energy gradient, calculated as in Eq. (23), is also plotted in both cases. The scaled magnitude of the magnetic moment in this case is $1.44 < M_I^F < 1.54\mu_B$, with an increase in magnitude as the angle moves away from its original value. The full magnetic moment is here $2.02 < M_I^{\mathrm{PAW}} < 2.13\mu_B$.

C. Discussion

1. Role of the magnetic moment magnitude

As shown in Fig. 1 our numerical results align well with the analytical conclusion in Eq. (20). In practice, this means accounting for the scaled magnitudes of the magnetic moments in Eq. (5), used when calculating the constraining fields. As a consequence, for a correct comparison, the energy gradient needs to be divided by the same magnitude of the magnetic moment. This appears to be a key difference between the approach in the present paper and that of Ref. [19]. The choice of magnetic moment magnitude to scale the energy gradient is, however, not uniquely defined. A detailed comparison of the various definitions, including their impact on the constraining fields, is provided in Sec. III C 4.

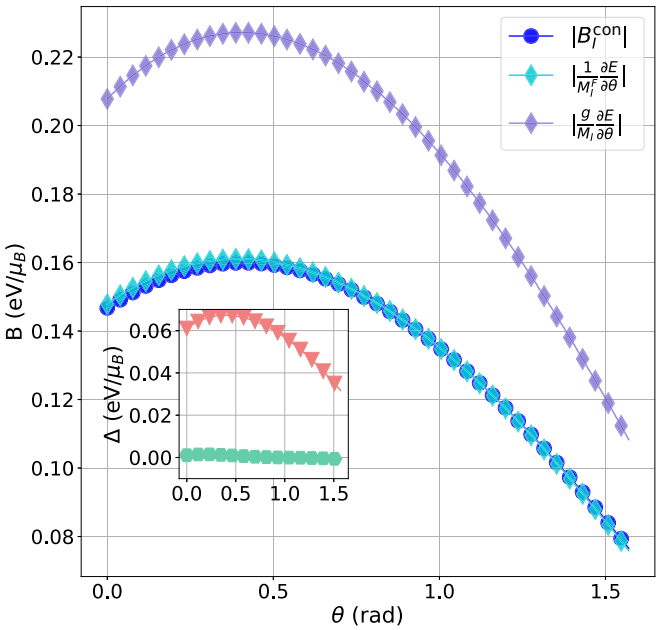


FIG. 3. Comparison of the constraining magnetic field and the effective magnetic field calculated as the energy derivative for the supercell of bcc Fe in disordered local moment background. The constraining field (blue circles) and effective magnetic field (turquoise diamonds) based on Eq. (21), with the magnetic moment magnitude M_l^F, agree well. The effective magnetic field of our data, but calculated differently, based on Eq. (23), shows a significant discrepancy (purple diamonds vs blue circles). The inset shows the difference between the two fields: $\Delta = |B_l^{\mathrm{eff}}| - |B_l^{\mathrm{con}}|$, where B_l^{eff} is given by either Eq. (21) [green hexagons] or (23) [orange triangles].

Furthermore, after accounting for the different magnetic moments, a second difference of an additional factor equal to (or very close to) 2 became apparent between our effective field and the one used in Fig. 2 of Ref. [19]. We speculate that this factor originates from the electron spin g factor indicated on the y axis of that figure. However, while Eq. (2) includes the g factor within the gyromagnetic ratio, it is not part of the effective magnetic field and, as best as we have been able to determine, the constraining field in VASP is not reported including this factor. As shown in Fig. 1, when we account for these differences our calculations reproduce the results of Ref. [19].

Our conclusion is thus that our derivation motivates adjusting the magnetic moment and g factor in the quantities used in the numerical comparison relative to those used in Ref. [19]. These adjustments reestablish the relationship between the effective field (obtained as the energy gradient) and the negative of the constraining field to match Eq. (20). The minor remaining discrepancy between these quantities in Fig. 2 can be explained by the numerical accuracy of the calculations.

Additionally, our results for both the Fe dimer and the bcc Fe supercell in a ferromagnetic background indicate that the discrepancy is unlikely to arise from the noncollinearity of the spin density, as the errors remain relatively consistent across the range of rotation angles. On the other hand, the behavior of the effective magnetic field calculated from the energy gradient, as expressed in Eq. (23), with increasing angle appear to show an increasingly larger discrepancy, which could be interpreted as arising from greater noncollinearity of the spin density as the system moves away from the collinear limit. However, this effect is more likely due to the difference in how we account for the magnetic moment magnitude when scaling the energy gradient in Eq. (23). This is particularly evident in the bcc Fe supercell in the ferromagnetic background, where the change in magnitude as the angle increases causes the constraining field and the energy gradient to respond differently. Specifically, the scaled magnetic moment (affecting the constraining field) decreases by 10%, while the full magnitude within the PAW potential sphere (affecting the energy gradient scaling) changes by only 6%. It is worth noting that the choice of the user-defined radius, when calculating the magnetic moment magnitude in cases (*i*) and (*ii*) from Sec. III B 2, significantly affects the discrepancy between the effective magnetic field derived from the energy gradient in Eq. (23) and the constraining field. Adjusting this radius can shift the constraining field curve closer to or further from this formulation of the energy gradient curve. Conversely, by scaling the energy gradient with the same magnetic moment magnitude used for the constraining field, this ambiguity is resolved, restoring the usual robustness of results across a range of radius values.

2. *Comparison of effective field expressions*

Supported by the presented numerical results, we now comment on some differences between our derivation of Eq. (22) and the part of the derivation in Ref. [19] that applies to SDFT. In our Eq. (11) the self-consistent effective potential is expressed for a constrained spin configuration, which contains a term due to the penalty energy. However, this term is not explicitly present in the corresponding expression of Eq. (6.11) in Ref. [19], which makes it unclear where the penalty energy contribution is accounted for in their derivation. The derivation in Ref. [19] states that the constraining field must be compared with the energy gradient of the total DFT energy, which is expressed in their Eq. (6.14) as

$$E_{\mathrm{DFT}} = \langle \hat{\mathcal{H}}_{\mathrm{KS}} \rangle + E_{\mathrm{dc}}, \tag{24}$$

where $\langle \hat{\mathcal{H}}_{\mathrm{KS}} \rangle$ is the sum of eigenvalues of the Kohn-Sham equations and E_{dc} is the so-called double counting term [19]. This would suggest that the term due to the penalty energy is not part of Eq. (24). However, Eq. (24) is obtained by expressing the single-particle kinetic energy as

$$T_0 = \langle \hat{\mathcal{H}}_{\mathrm{KS}} \rangle - \sum_{\alpha\beta} \int v_{\alpha\beta}^{\mathrm{eff}}(\mathbf{r}) n_{\beta\alpha}(\mathbf{r}) d\mathbf{r} \tag{25}$$

and replacing it in Eq. (7) (cf. Refs. [30] or [39]). When considering our expression in Eq. (11) for $\mathbf{v}^{\mathrm{eff}}(\mathbf{r})$, this expression for the total DFT energy incorporates the effect of the constraining field. As a result, Eq. (24), i.e., the expression used in Ref. [19] for E_{DFT}, does not correspond to our energy E_0 in, e.g., Eq. (20), which appears to be a mismatch between the quantities representing the effective field in the two derivations. Furthermore, it is described in Ref. [19] that their constraining field theorem is applied to the Kohn-Sham Hamiltonian. A possible interpretation of this is that the derivation includes a constraining-field term in the expression

for the effective potential. However, if that is the case, we again arrive at the same conclusion that E_{DFT}, as described by Eq. (24) above, is not equal to our E_0, in contrast to the implications of Eq. (7.1) in Ref. [19].

3. Comment on tight-binding model and the magnetic force theorem

In the work by Streib *et al.*, a numerical investigation based on a mean-field tight-binding model is conducted in addition to the DFT investigation [19]. In this case, the Hamiltonian contains a Stoner term that depends on the input magnetization direction. As pointed out by the authors, this term will make the magnetic moments approximately align with the desired direction. However, to ensure that they are completely aligned, constraining fields are added. Here, we believe there is an important distinction from the SDFT case outlined previously. The constraining fields in this tight-binding example serve to correct for the insufficiency of rotating only the input Stoner field. Consequently, the two contributions to the rotation of the magnetization can be separated and the difference can be plotted between the compensating constraining field and the change in energy due to the rotation of the Stoner term in Fig. 4 of Ref. [19].

Considering the DFT adaptation of the constraining field theorem given by Eq. (6.15) of Ref. [19], the fact that the magnetic force theorem (MFT) is utilized in this derivation suggests an interpretation in which the exchange-correlation field is manually rotated, hence playing the same role as the Stoner term in the mean-field tight-binding model example described above. Within the MFT-based formalism of extracting exchange interaction parameters [40], one assumes that rotating the exchange-correlation field yields the rotated magnetization and, subsequently, the energy difference. This is, however, an approximation, since the rotated input exchange-correlation potential and the output magnetization density, after solving the Kohn-Sham equations, will not be collinear; collinearity only holds at true equilibrium [12,41,42]. By this interpretation, the role of the constraining field in Eq. (6.15) of Ref. [19] could be viewed as compensating for the insufficiency of rotating the exchange correlation field within the MFT formalism. However, as demonstrated in this work, this is not the role of the constraining field in SDFT, where the constraining fields generate torques that exactly cancel out the internal torques, bringing the system to a stationary quasiequilibrium state. Furthermore, as demonstrated by Solovyev, the same holds in linear response theory; with an exact treatment of the total energy change, i.e., including the constraining field, the internal torques are exactly canceled out by the constraining field [42,43].

4. Magnetic moment definitions and constraining field scaling

The choice of magnetic moment magnitude used to scale the energy gradient is crucial. Dividing by M_I^F is not physically justified, since the function $F(|\mathbf{r}-\mathbf{r}_I|)$, while introduced for mathematical robustness, does not reflect any underlying physical reality. Hence the energy gradient should be divided by the full magnetic moment. Consequently, the constraining field must be rescaled to also reflect the torque on the full magnetic moment. We will return to this later;

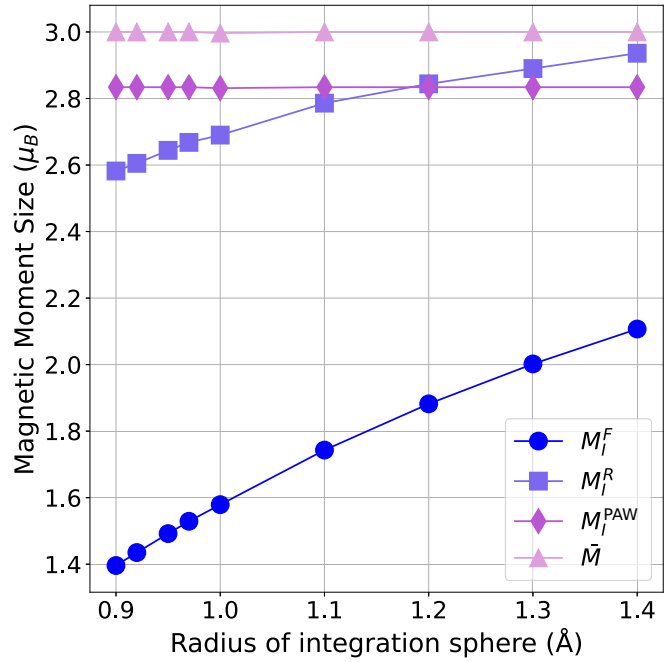


FIG. 4. Magnitude of the atomic magnetic moment of a ferromagnetic Fe dimer as a function of the user-defined integration sphere radius. M_I^F, M_I^R, and M_I^{PAW} are defined in Sec. III B 2. $\bar{M}$ is the average magnitude of the atomic magnetic moment when integrating over the whole simulation cell.

first, we investigate how to define the full magnetic moment, which is not uniquely determined due to its dependence on the user-defined radius of the integration sphere. The variation of the magnitude of the magnetic moment in the dimer with respect to the radius is presented in Fig. 4, when both moments are in the same direction. We include the magnetic moment given by integrating over the whole simulation cell and divide it by 2, denoted as $\bar{M}$. Neither M_I^{PAW} nor $\bar{M}$ depend on the user-defined radius. At a radius of 1 Å, the magnitudes M_I^R and M_I^{PAW} differ by approximately $0.14\mu_{\mathrm{B}}$; the difference between M_I^R and $\bar{M}$ is approximately $0.31\mu_{\mathrm{B}}$. The variation in M_I^F with changing radius is considerably larger compared to M_I^R. This is also reflected in how the constraining field varies with the user-defined radius. Figure 5 shows the constraining field as a function of the radius when the constraining field is directly obtained from the output of VASP and the two cases when $|B_I^{\mathrm{con}}|$ is scaled by M_I^F/M_I^R and M_I^F/M_I^{PAW}, respectively. The constraining field in Fig. 5 is obtained when the two magnetic moments of the dimer are at a 90° angle relative to each other. By rescaling the constraining field with the full magnetic moment size, the strong user-defined radius dependence is quenched significantly.

Now, to ensure that rescaling the constraining field is equivalent to dividing the energy gradient by the full magnetic moment, we compare the two in Fig. 6. As seen, the energy gradient and the scaled constraining field follow each other nicely. To calculate the correct physical torque on the magnetic moment, the scaled constraining field should be used, since we are after the torque on the full magnetic moment, not on the magnetic moment reduced by the function $F(|\mathbf{r}-\mathbf{r}_I|)$. The exact definition of the full magnetic moment is to some

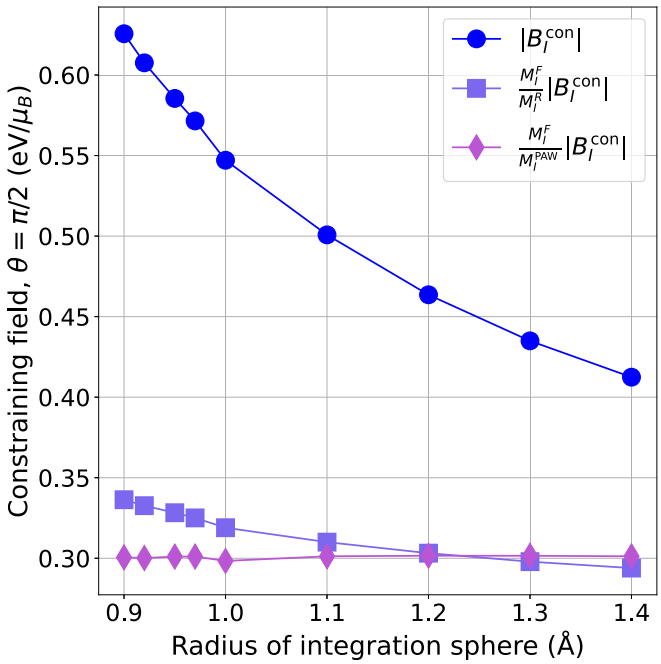


FIG. 5. Magnitude of the bare constraining field $\mathbf{B}_I^{\text{con}}$ and when rescaled by the full magnetic moment defined as M_I^R and M_I^{PAW}, respectively, of an Fe dimer. The two magnetic moments are in a 90° angle relative to each other.

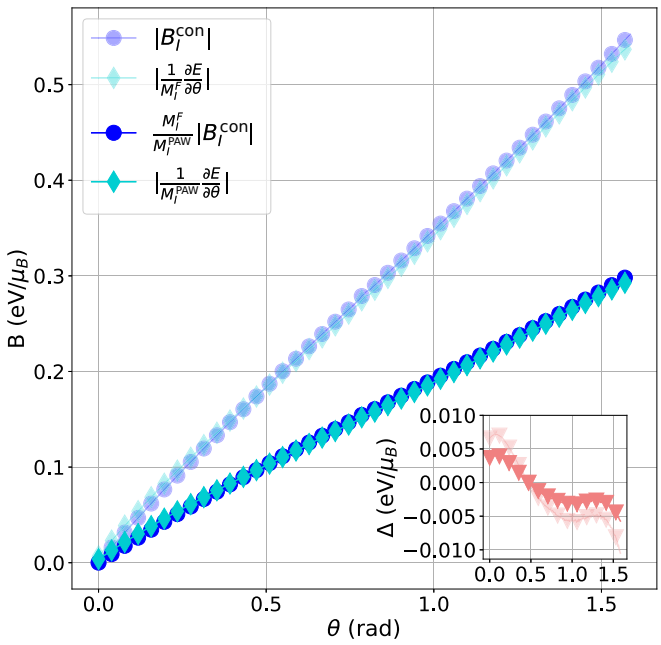


FIG. 6. Comparison of the constraining field and the effective magnetic field calculated as the energy derivative for the Fe dimer. The faint circles and diamonds correspond to the same result as in Fig. 1. The bold blue circles and turquoise diamonds show the rescaled constraining field and the energy derivative divided by the full magnetic moment, respectively. The inset shows the difference between the two fields with (bold triangles) and without rescaling (faint triangles); $\Delta = |B_I^{\text{eff}}| - |B_I^{\text{con}}|$, where B_I^{eff} is given by Eq. (21).

extent ambiguous. In practice, however, the results are robust across a reasonable range of sphere radii. In Fig. 6 we use the PAW sphere moment, M_I^{PAW}, as a natural and consistent choice. As indicated by Fig. 5, a user-defined sphere radius within a range of radii (1.1–1.4 Å) would lead to very similar results.

IV. CONCLUSIONS

In this work, we have revisited the derivation of the relationship between the effective and constraining fields in constrained SDFT from Ref. [16] and performed numerical investigations of an Fe dimer and supercells of bcc Fe in both ferromagnetic and magnetically disordered backgrounds. We show analytically that when the penalty term is properly included within the total energy functional of constrained SDFT and the resulting Kohn-Sham equations, the constraining fields exactly cancel the internal torques. This resolves the apparent discrepancy reported in the analytical derivation of Ref. [19]. We also discuss how this situation differs when employing a tight-binding model with a Stoner term and clarify the role of constraining fields in that case. In the numerical investigation, we find that adjusting the quantities used in Ref. [19] allows us to reestablish that the effective magnetic fields derived from the energy gradient are equal to the negative of the constraining field. We attribute the contrast between our numerical findings and those of Ref. [19] to differences in the quantities used when calculating the constraining field and the effective field given by the energy gradient in relation to the magnetic moment magnitude and the g factor. We show how the full and physically meaningful magnetic moment can be defined either by integrating over a user defined atomic sphere or the PAW potential sphere. In addition, it is described how the constraining fields can be rescaled to describe the effective field acting on this complete magnetic moment. Hence we conclude that, within the framework of SDFT, constraining fields can be utilized to efficiently calculate the torques that act on magnetic moments in adiabatic *ab initio* spin dynamics.

ACKNOWLEDGMENTS

The computations were enabled by resources provided by the National Academic Infrastructure for Supercomputing in Sweden (NAISS), partially funded by the Swedish Research Council through Grant Agreement No. 2022-06725. B.A. acknowledges financial support from the Swedish Research Council (VR) through Grants No. 2019-05403 and No. 2023-05194 and from the Swedish Government Strategic Research Area in Materials Science on Functional Materials at Linköping University (Faculty Grant SFOMatLiU No. 2009-00971). R.A. acknowledges financial support from the Swedish Research Council (VR) Grant No. 2020-05402 and the Swedish e-Science Research Centre (SeRC).

DATA AVAILABILITY

The data that support the findings of this article are not publicly available. The data are available from the authors upon reasonable request.

[1] E. Beaurepaire, J.-C. Merle, A. Daunois, and J.-Y. Bigot, Ultrafast spin dynamics in ferromagnetic nickel, Phys. Rev. Lett. **76**, 4250 (1996).

[2] T. J. Penfold, J. O. Johansson, and J. Eng, Towards understanding and controlling ultrafast dynamics in molecular photomagnets, Coord. Chem. Rev. **494**, 215346 (2023).

[3] A. Bergman, B. Skubic, J. Hellsvik, L. Nordström, A. Delin, and O. Eriksson, Ultrafast switching in a synthetic antiferromagnetic magnetic random-access memory device, Phys. Rev. B **83**, 224429 (2011).

[4] G. Venkat, D. A. Allwood, and T. J. Hayward, Magnetic domain walls: Types, processes and applications, J. Phys. D: Appl. Phys. **57**, 063001 (2024).

[5] O. Eriksson, A. Bergman, L. Bergqvist, and J. Hellsvik, *Atomistic Spin Dynamics: Foundations and Applications*, first ed. (Oxford University Press, Oxford, 2017).

[6] H. Zhang, Y. Zhang, Z. Hou, M. Qin, X. Gao, and J. Liu, Magnetic skyrmions: Materials, manipulation, detection, and applications in spintronic devices, Mater. Futures **2**, 032201 (2023).

[7] V. P. Antropov, M. I. Katsnelson, M. van Schilfgaarde, and B. N. Harmon, *Ab initio* spin dynamics in magnets, Phys. Rev. Lett. **75**, 729 (1995).

[8] V. P. Antropov, M. I. Katsnelson, B. N. Harmon, M. van Schilfgaarde, and D. Kusnezov, Spin dynamics in magnets: Equation of motion and finite temperature effects, Phys. Rev. B **54**, 1019 (1996).

[9] I. Stockem, A. Bergman, A. Glensk, T. Hickel, F. Körmann, B. Grabowski, J. Neugebauer, and B. Alling, Anomalous phonon lifetime shortening in paramagnetic CrN caused by spin-lattice coupling: A combined spin and *ab initio* molecular dynamics study, Phys. Rev. Lett. **121**, 125902 (2018).

[10] D. Gambino, J. Klarbring, and B. Alling, Phase stability of Fe from first principles: Atomistic spin dynamics coupled with *ab initio* molecular dynamics simulations and thermodynamic integration, Phys. Rev. B **107**, 014102 (2023).

[11] M. Arale Brännvall, D. Gambino, R. Armiento, and B. Alling, Machine learning approach for longitudinal spin fluctuation effects in bcc Fe at T_c and under Earth-core conditions, Phys. Rev. B **105**, 144417 (2022).

[12] G. M. Stocks, B. Ujfalussy, X. Wang, D. M. C. Nicholson, W. A. Shelton, Y. Wang, A. Canning, and B. L. Györffy, Towards a constrained local moment model for first principles spin dynamics, Philos. Mag. B **78**, 665 (1998).

[13] K. Capelle, G. Vignale, and B. L. Györffy, Spin currents and spin dynamics in time-dependent density-functional theory, Phys. Rev. Lett. **87**, 206403 (2001).

[14] K. Capelle and B. L. Gyorffy, Exploring dynamical magnetism with time-dependent density-functional theory: From spin fluctuations to Gilbert damping, Europhys. Lett. **61**, 354 (2003).

[15] P. H. Dederichs, S. Blügel, R. Zeller, and H. Akai, Ground states of constrained systems: Application to cerium impurities, Phys. Rev. Lett. **53**, 2512 (1984).

[16] D. M. Edwards, On the dynamics of itinerant electron magnets in the paramagnetic state, J. Magn. Magn. Mater. **45**, 151 (1984).

[17] B. Újfalussy, X.-D. Wang, D. M. C. Nicholson, W. A. Shelton, G. M. Stocks, Y. Wang, and B. L. Gyorffy, Constrained density functional theory for first principles spin dynamics, J. Appl. Phys. **85**, 4824 (1999).

[18] P.-W. Ma and S. L. Dudarev, Constrained density functional for noncollinear magnetism, Phys. Rev. B **91**, 054420 (2015).

[19] S. Streib, V. Borisov, M. Pereiro, A. Bergman, E. Sjöqvist, A. Delin, O. Eriksson, and D. Thonig, Equation of motion and the constraining field in *ab initio* spin dynamics, Phys. Rev. B **102**, 214407 (2020).

[20] G. Kresse and J. Hafner, *Ab initio* molecular dynamics for liquid metals, Phys. Rev. B **47**, 558 (1993).

[21] G. Kresse and J. Hafner, *Ab initio* molecular-dynamics simulation of the liquid-metal–amorphous-semiconductor transition in germanium, Phys. Rev. B **49**, 14251 (1994).

[22] G. Kresse and J. Furthmüller, Efficiency of *ab-initio* total energy calculations for metals and semiconductors using a plane-wave basis set, Comput. Mater. Sci. **6**, 15 (1996).

[23] G. Kresse and J. Furthmüller, Efficient iterative schemes for *ab initio* total-energy calculations using a plane-wave basis set, Phys. Rev. B **54**, 11169 (1996).

[24] S. Streib, A. Szilva, V. Borisov, M. Pereiro, A. Bergman, E. Sjöqvist, A. Delin, M. I. Katsnelson, O. Eriksson, and D. Thonig, Exchange constants for local spin Hamiltonians from tight-binding models, Phys. Rev. B **103**, 224413 (2021).

[25] S. Streib, R. Cardias, M. Pereiro, A. Bergman, E. Sjöqvist, C. Barreteau, A. Delin, O. Eriksson, and D. Thonig, Adiabatic spin dynamics and effective exchange interactions from constrained tight-binding electronic structure theory: Beyond the Heisenberg regime, Phys. Rev. B **105**, 224408 (2022).

[26] R. Cardias, S. Streib, Z. Lu, M. Pereiro, A. Bergman, E. Sjöqvist, C. Barreteau, A. Delin, O. Eriksson, and D. Thonig, Coupled spin-lattice dynamics from the tight-binding electronic structure, Phys. Rev. B **109**, 144303 (2024).

[27] T. Gilbert, A phenomenological theory of damping in ferromagnetic materials, IEEE Trans. Magn. **40**, 3443 (2004).

[28] T. Yang, Z. Cai, Z. Huang, W. Tang, R. Shi, A. Godfrey, H. Liu, Y. Lin, C.-W. Nan, M. Ye, L. F. Zhang, K. Wang, H. Wang, and B. Xu, Deep learning illuminates spin and lattice interaction in magnetic materials, Phys. Rev. B **110**, 064427 (2024).

[29] U. von Barth and L. Hedin, A local exchange-correlation potential for the spin polarized case. I, J. Phys. C **5**, 1629 (1972).

[30] J. Kübler, *Theory of Itinerant Electron Magnetism* (Oxford University Press, Oxford, Great Britain, 2000).

[31] P. E. Blöchl, Projector augmented-wave method, Phys. Rev. B **50**, 17953 (1994).

[32] G. Kresse and D. Joubert, From ultrasoft pseudopotentials to the projector augmented-wave method, Phys. Rev. B **59**, 1758 (1999).

[33] J. P. Perdew, K. Burke, and M. Ernzerhof, Generalized gradient approximation made simple, Phys. Rev. Lett. **77**, 3865 (1996).

[34] H. J. Monkhorst and J. D. Pack, Special points for Brillouin-zone integrations, Phys. Rev. B **13**, 5188 (1976).

[35] B. Alling, T. Marten, and I. A. Abrikosov, Effect of magnetic disorder and strong electron correlations on the thermodynamics of CrN, Phys. Rev. B **82**, 184430 (2010).

[36] B. L. Gyorffy, A. J. Pindor, J. Staunton, G. M. Stocks, and H. Winter, A first-principles theory of ferromagnetic phase transitions in metals, J. Phys. F: Met. Phys. **15**, 1337 (1985).

[37] A. Savitzky and M. J. E. Golay, Smoothing and differentiation of data by simplified least squares procedures, Anal. Chem. **36**, 1627 (1964).

[38] P. Virtanen, R. Gommers, T. E. Oliphant, M. Haberland, T. Reddy, D. Cournapeau, E. Burovski, P. Peterson, W. Weckesser, J. Bright, S. J. van der Walt, M. Brett, J. Wilson, K. J. Millman, N. Mayorov, A. R. J. Nelson, E. Jones, R. Kern, E. Larson, C. J. Carey, *et al.*, SciPy 1.0: Fundamental algorithms for scientific computing in python, Nat. Methods **17**, 261 (2020).

[39] R. Martin, *Electronic Structure: Basic Theory and Practical Methods* (Cambridge University Press, Cambridge, UK, 2020).

[40] A. Liechtenstein, M. Katsnelson, V. Antropov, and V. Gubanov, Local spin density functional approach to the theory of exchange interactions in ferromagnetic metals and alloys, J. Magn. Magn. Mater. **67**, 65 (1987).

[41] P. Bruno, Exchange interaction parameters and adiabatic spin-wave spectra of ferromagnets: A "*renormalized* magnetic force theorem", Phys. Rev. Lett. **90**, 087205 (2003).

[42] I. V. Solovyev, Exchange interactions and magnetic force theorem, Phys. Rev. B **103**, 104428 (2021).

[43] I. V. Solovyev, Linear response theories for interatomic exchange interactions, J. Phys.: Condens. Matter **36**, 223001 (2024).